Monthly Notices
of the
ROYAL ASTRONOMICAL SOCIETY

Mon. Not. R. Astron. Soc. **419,** 1860–1870 (2012) doi:10.1111/j.1365-2966.2011.19840.x

A newly discovered young massive star cluster at the far end of the Galactic Bar

Ben Davies,[1,2⋆] Diego de la Fuente,[3] Francisco Najarro,[3] Jim A. Hinton,[4] Christine Trombley,[5] Donald F. Figer[5] and Elena Puga[3,6]

[1]*Institute of Astronomy, University of Cambridge, Madingley Road, Cambridge CB3 0HA*
[2]*School of Physics and Astronomy, University of Leeds, Woodhouse Lane, Leeds LS2 9JT*
[3]*Centro de Astrobiologia (INTA/CSIC), Instituto Nacional de Tecnica Aeroespacial, Ctra. de Ajalvir, km 4, 28850 Torrejon de Ardoz, Madrid, Spain*
[4]*Department of Physics and Astronomy, University of Leicester, Leicester LE1 7RH*
[5]*Center for Detectors, Rochester Institute of Technology, 54 Lomb Memorial Drive, Rochester, NY 14623, USA*
[6]*Herschel Science Centre, European Space Astronomy Centre, PO Box 78, 28691 Villanueva de la Cañada, Madrid, Spain*

Accepted 2011 September 16. Received 2011 September 15; in original form 2011 August 9

ABSTRACT

We present a near-infrared study of the candidate star cluster Mercer 81, located at the centre of the G338.4+0.1 H II region and close to the TeV gamma-ray source HESS 1640–465. Using *Hubble Space Telescope*/NICMOS imaging and VLT/ISAAC spectroscopy, we have detected a compact and highly reddened cluster of stars, although the bright stars in the centre of the field are in fact foreground objects. The cluster contains nine stars with strong Pα emission, one of which we identify as a Wolf–Rayet (WR) star, as well as an A-type supergiant. The line-of-sight extinction is very large, $A_V \sim 45$, illustrating the challenges of locating young star clusters in the Galactic plane. From a quantitative analysis of the WR star, we argue for a cluster age of $3.7^{+0.4}_{-0.5}$ Myr, and, assuming that all emission-line stars are WR stars, a cluster mass of $\gtrsim 10^4\,M_\odot$. A kinematic analysis of the cluster's surrounding H II region shows that the cluster is located in the Galactic disc at a distance of 11 ± 2 kpc. This places the cluster close to where the far end of the Bar intersects the Norma spiral arm. This cluster, as well as the nearby cluster [DBS2003]179, represents the first detections of active star cluster formation at this side of the Bar, in contrast to the near side which is well known to have recently undergone a $\sim 10^6\,M_\odot$ starburst episode.

Key words: stars: Wolf–Rayet – ISM: clouds – H II regions – open clusters and associations: general – open clusters and associations: individual: Mercer 81.

1 INTRODUCTION

Young massive star clusters (YMCs; ages $\lesssim 50$ Myr and masses $\gtrsim 10^4\,M_\odot$) have relevance to many areas of astrophysics. They contain large numbers of massive stars, whose high temperatures, high luminosities, dense winds and supernova explosions make YMCs a considerable source of mechanical energy, ionizing radiation and chemically processed ejecta. The effect that they have on their surroundings is profound, clearing away the remains of their natal molecular cloud, whilst revealing and triggering subsequent generations of star formation (e.g. González Delgado & Pérez 2000; Smith 2006; Davies, Clark & Others 2011a; De Marchi et al. 2011). Their large populations of massive stars make them ideal natural laboratories with which to study the evolution of massive stars up to supernova and beyond (e.g. Martins et al. 2007, 2008; Bibby et al. 2008; Davies et al. 2008, 2009). Finally, they can dominate the radiative output of their host galaxies, either through direct ultraviolet and optical emission or through reprocessed emission in the form of ionized gas or heated dust (Alonso-Herrero et al. 2002).

Our knowledge of our own Galaxy's population of YMCs is extremely incomplete, in stark contrast to external galaxies (e.g. Bastian et al. 2005; Konstantopoulos et al. 2009). The high levels of interstellar extinction in the plane of the Galaxy have meant that until recently very few clusters were known beyond a distance of $\sim$1 kpc. Most known clusters beyond this distance were found by targeted searches of, for example, the Galactic Centre (Cotera et al. 1996; Figer et al. 1999), giant H II regions (Blum, Damineli & Conti 1999; Blum, Conti & Damineli 2000; Blum, Damineli & Conti 2001), fields around newly born neutron stars (Fuchs et al. 1999; Vrba et al. 2000), or simply because the foreground extinction was low enough to detect the cluster at optical wavelengths (Westerlund 1987). However, recent infrared (IR) surveys of the Galactic plane,

⋆E-mail: bdavies@ast.cam.ac.uk

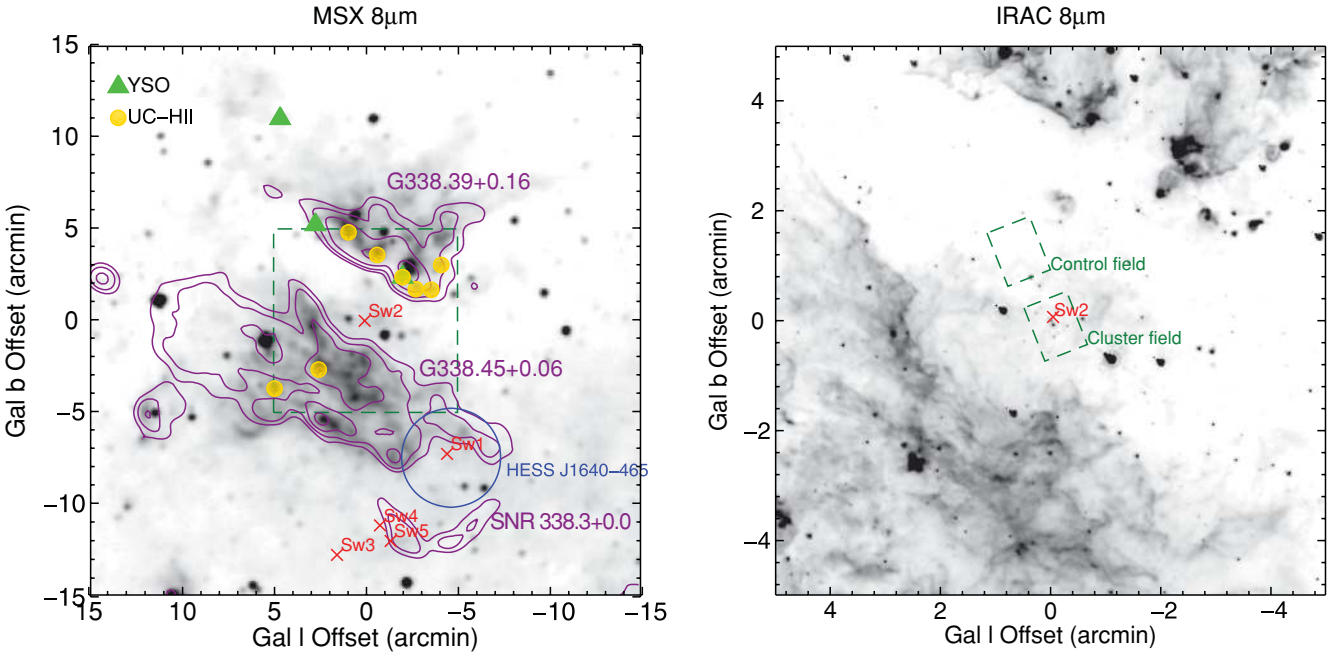

Figure 1. Wide-field images of Mc81 and its surroundings. Left: the *MSX* 8-μm image, which shows the diffuse nebula surrounding the cluster. The locations of *Swift* X-ray sources (Landi et al. 2006), as well as the location of the TeV emission source HESS J1640–465, are indicated. The contours indicate the morphology of the 843-MHz emission (Bock et al. 1999), and the dashed green box shows the field of view of the right-hand panel. Right: a higher resolution 8-μm image from the GLIMPSE survey. The brightest stars of the cluster are coincident with the X-ray source Sw 2. The NICMOS cluster and control fields of view are illustrated by the dashed green boxes.

beginning with 2MASS (Skrutskie et al. 2006), and more recently *Spitzer*/GLIMPSE (Benjamin et al. 2003) and VVV (Minniti et al. 2010), are finally helping us to uncover the cluster population of the Galactic disc and affording the opportunity to search the Galactic plane for clusters in a systematic way.

By-eye and algorithmic searches of survey data (e.g. Ivanov et al. 2002; Dutra et al. 2003; Mercer et al. 2005; Froebrich, Scholz & Raftery 2007; Borissova et al. 2011) have yielded over 1000 candidates for newly discovered star clusters. However, such catalogues inevitably contain large numbers of false positives, due to chance alignments of stars, patchy foreground extinction and spatially extended emission incorrectly classified as unresolved star clusters. Therefore, these catalogues of candidates must be analysed carefully using multiwavelength survey data and, ultimately, follow-up spectroscopic observations before their distances and physical properties may be derived (e.g. Kurtev et al. 2007; Messineo et al. 2009; Hanson et al. 2010). Only then can they be placed in the framework of the Galaxy's recent star-forming history.

One such candidate is object #81 from the catalogue of Mercer et al. (2005), known hereafter as Mc81.[1] This object was found in an algorithmic search of the GLIMPSE survey, by looking for spatial groups of stars with similar photometric properties. The clues to its nature, however, come from cross-correlation with other data in the literature. The object appears to be at the centre of the H II region G338.4+0.1, a bubble of warm dust and ionized gas, visible in the SUMSS 843-MHz (Bock, Large & Sadler 1999) and *MSX* 8-μm (Price et al. 2001) images, and in more detail in the GLIMPSE 8-μm image (Fig. 1). The object's location is close to a supernova remnant (SNR) as found by Green (2004) from the 'shell' morphology of continuum radio emission, but with no spectral index measurement the object could also be a wind-blown bubble.

Close to the centre of the SNR is a high-energy TeV gamma-ray source, HESS J1640–465 (Aharonian et al. 2005), at a distance of 8 arcmin (a linear distance of 22 pc, if the complex is at a distance of 11 kpc – see Section 3.3). This source, as with many other TeV sources, is thought to be associated with a pulsar wind nebula (Funk et al. 2007), indicative of recent SN activity. Indeed, TeV emission can be a useful tracer of massive star formation in the Galactic plane as it is unaffected by absorption, and there are other YMCs in the literature that are known to be associated with such sources as RSGC1 (Figer et al. 2006; Davies et al. 2008), Cl 1813–178 (Messineo et al. 2008) and Westerlund 2 (Aharonian et al. 2007). Finally, in a follow-up of HESS J1640–465, a number of hard X-ray sources were detected in the field of Mc81, with one source being perfectly aligned with the cluster (see right-hand panel of Fig. 1; Landi et al. 2006). Such emission could be explained by either a recently formed neutron star or a colliding wind binary, with both explanations being indicators of youth (for an analysis of the X-ray emission from another young star cluster, Westerlund 1, see Clark et al. 2008).

Based on this evidence we have carried out extensive follow-up observations of Mc81 with near-infrared (NIR) photometry and spectroscopy, with a view to confirm that the object is indeed a young star cluster and ultimately to determine the cluster's physical properties.

In Section 2, we present description of the observations, data reduction and analysis steps. In Section 3 we describe our results and show that the object is indeed a highly reddened star cluster, and estimate its age and mass. We summarize our results in Section 5.

[1] Objects in this catalogue are referred to by some authors with the prefix GLIMPSE, e.g. *GLIMPSE81*.

Table 1. Read sequences and total integration times employed for each filter during the NICMOS observations.

Filter	SAMP-SEQ	NSAMP	$T_{\rm int}$ (s)
F160W	STEP2	15	144
F222M	STEP8	12	336
F187N	STEP8	10	240
F190N	STEP8	10	240

2 OBSERVATIONS AND DATA REDUCTION

2.1 Imaging

Images were obtained with *Hubble Space Telescope* (*HST*)/NICMOS on 2008 October 22, as part of observing programme #11545 (PI: B. Davies). We used the NIC3 camera which has a field of view of 51.2× 51.2 arcsec^2 and a pixel scale of 0.2 arcsec. We observed the cluster through filters *F*160*W* and *F*222*M*, as well as the narrow-band filters *F*187*N* and *F*190*N* which are centred on Pα and the neighbouring continuum, respectively. In addition to the cluster we observed a nearby control field through the *F*160*W* and *F*222*M* filters in order to characterize the foreground population. The fields of observation are indicated in Fig. 1.

Our observations used a spiral dither pattern with six pointings with offset distance set to 5.07 arcsec. This subpixel dithering technique was designed to minimize the impact of non-uniform intrapixel sensitivity on our photometry. We used MULTIACCUM readout modes, as well as the sampling sequences and total integration times listed in Table 1.

Our reduction procedure followed the guidelines of the NICMOS Data Handbook v7.0. The standard reduction steps of bias subtraction, dark-current correction and flat-fielding were performed using CALNICA. Before mosaicking, each dithered observation was subsampled on to a 3× finer grid using bilinear interpolation to account for the subpixel dithering.

Photometry was extracted from the images using the STARFINDER package which run within IDL (Diolaiti et al. 2000), in conjunction with point spread functions (PSFs) which were computed for each filter using TINYTIM. STARFINDER uses these PSFs to locate stars within each image, and we employed two iteration cycles to fine-tune the astrometry and photometry. Since our fields of observation are not very crowded, we did not use the deblending algorithm, as this was found to produce many false detections. Uncertainties and completeness limits were determined by inserting fake stars into each image and measuring the recovery rate.

2.2 Spectroscopy

Spectroscopic data were taken on the nights of 2009 April 11 and 2009 May 4 as part of European Southern Observatory's (ESO) observing programme 083.D-0765(A) (PI: E. Puga), using the ISAAC spectrograph on the VLT (Moorwood et al. 1998) in 'medium' resolution mode. Our targets were the stars labelled '1' and '3' in Fig. 2, which were determined to be likely cluster members based on their photometric properties (see later). We used the 0.8-arcsec slit at three different central wavelengths – 1.71, 2.09 and 2.21 μm – providing a spectral resolution of $\Delta\lambda/\lambda \sim 4000$. The DIT × NDIT × NINT combination for each wavelength setting was (8 × 8 × 30 s), (8 × 8 × 32 s) and (16 × 8 × 24 s), respectively. The observations were taken in a ABBA pattern to isolate and subtract sky emission features. In addition to the target stars we observed the B9 v stars Hip090248 and Hip091286 as measures of the telluric absorption, as well as the usual observations of flat-fields, dark frames and arcs for wavelength calibration. To characterize the spatial distortion, a bright field star was stepped along the slit and re-observed multiple times.

The data reduction procedure began with the subtraction of nod pairs to remove sky emission, and division by a normalized flat-field. The 2D frames were then rectified on to an orthogonal grid, using the stepped-star and arc frames to characterize the distortion in the spatial and dispersion directions, respectively. This process also wavelength-calibrates the data, with rms residuals which were

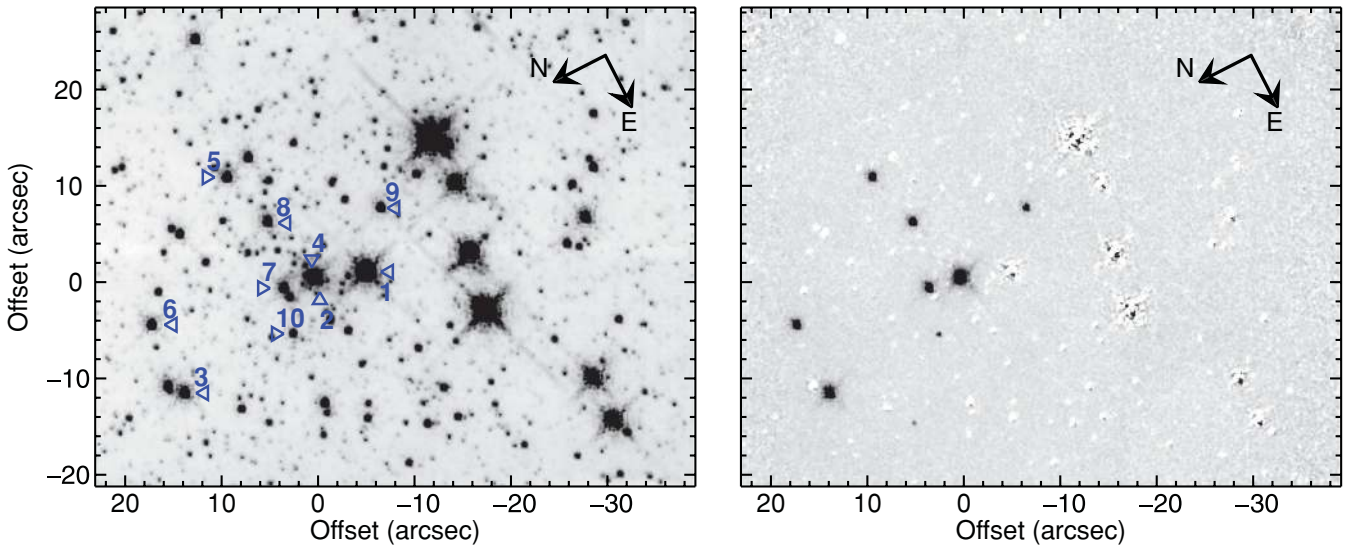

Figure 2. NICMOS images of the cluster. Left: image of the cluster taken through the *F*222*M* filter. The two stars for which we have spectra, as well as the other emission-line stars, are indicated by the blue triangles. Right: the difference image (*F*187*N* − *F*190*N*), which highlights the emission-line stars. The arrows in the top right of each image indicate the orientation.

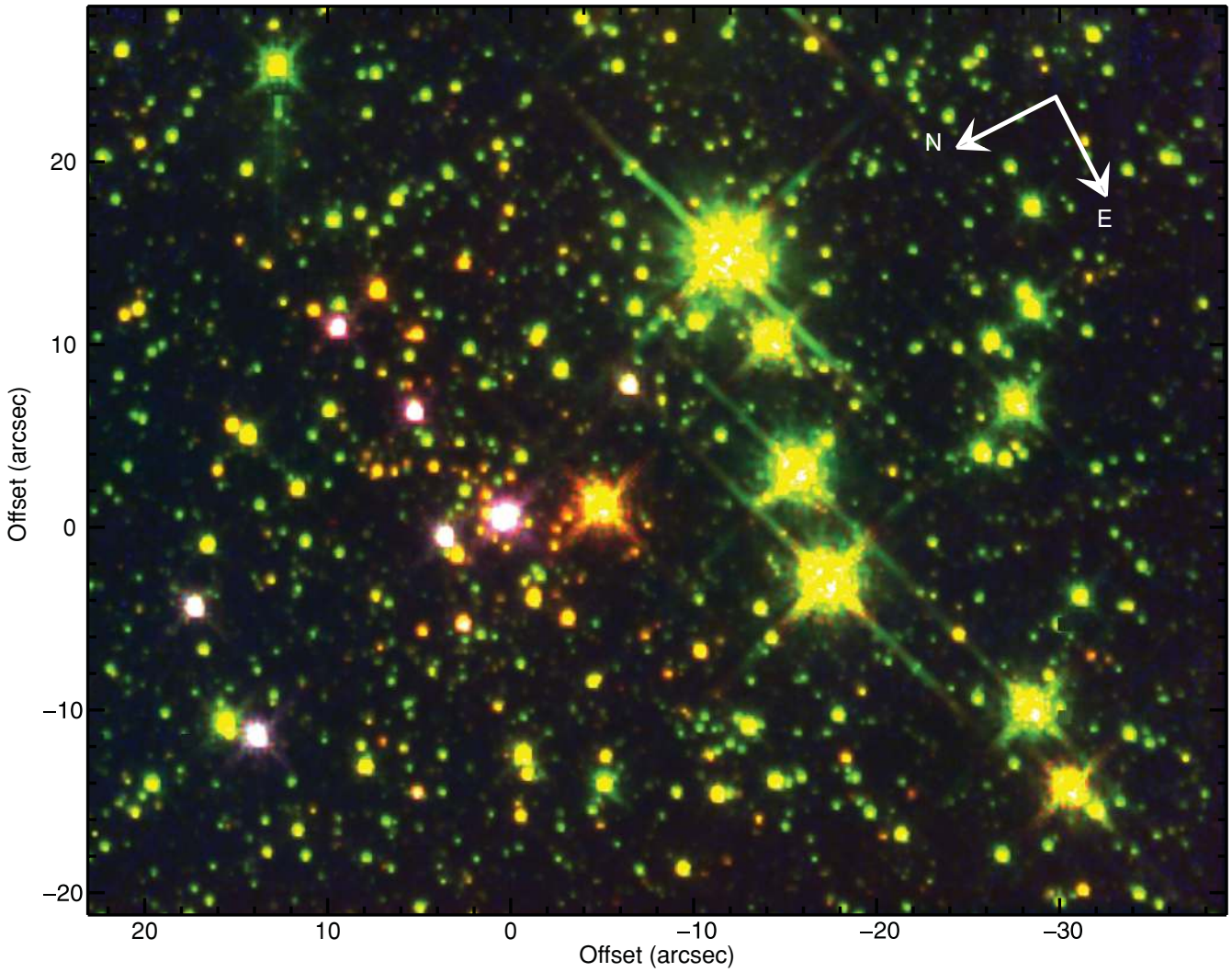

Figure 3. Three-colour image of the cluster from the NICMOS data, with colours as follows: R, F222M; G, F160W; B, $F187N - F190N$. Therefore, the highly reddened cluster stars appear red/orange, and the cluster's emission-line stars appear pink/magenta.

found to be less than a tenth of a resolution element ($\sim$10 km s^{-1}). After rectification, the spectra were extracted and combined.

The telluric standard spectra had their intrinsic H I absorption removed by fitting the lines with Voigt profiles. The telluric spectra were then cross-correlated with the target spectra in the region of isolated telluric features to correct for any residual subpixel shifts, before the target spectra were divided by the telluric spectra.

3 RESULTS AND ANALYSIS

3.1 Photometry

The NICMOS images of Mc81 can be seen in Fig. 2. The left-hand panel shows the F222M image of the cluster. In the right-hand panel, we show the difference image [F187N − F190N], which clearly highlights nine stars with significant Pα emission.[2] This strongly suggests that these are hot stars with strong winds, and are therefore likely to have ages of $\lesssim$10 Myr.

In Fig. 3 we show a three-colour RGB image of F222M (red), F160W (green) and [F187N−F190N] (blue). Around the coordinate centre, a group of highly reddened stars is clearly seen, that form the putative cluster. In this colour scheme, the emission-line stars, which are also heavily reddened, are shown by pink/magenta. From these data, there is already strong evidence for a young, highly reddened cluster of stars in the field of Mc81. The four bright stars to the south of the cluster have a green/yellow colour, indicating that they are in the foreground. Ironically, it is likely that these four stars in part triggered the cluster detection algorithm used by Mercer et al. (2005). These authors claim that they detected an association of 65 stars, although the positions of these stars are not listed, so it is not possible for us to check whether the cluster detected by Mercer et al.'s algorithm bears any relation to the cluster we describe here. For the sake of clarity and consistency, we continue to refer to the cluster studied in this work as Mc81.

The results of the NICMOS photometry are shown in Fig. 4. The left-hand panel shows a colour–magnitude diagram of the stars within 18 arcsec of the cluster centre, which we define as the location of the brightest emission-line star. Also shown in the plot are data from an area in the control field of identical size. There is an obvious difference between the two regions, with the 'cluster' field showing

[2] It is possible that He II emission contributes to the flux in this band, especially if the stars are WR stars.

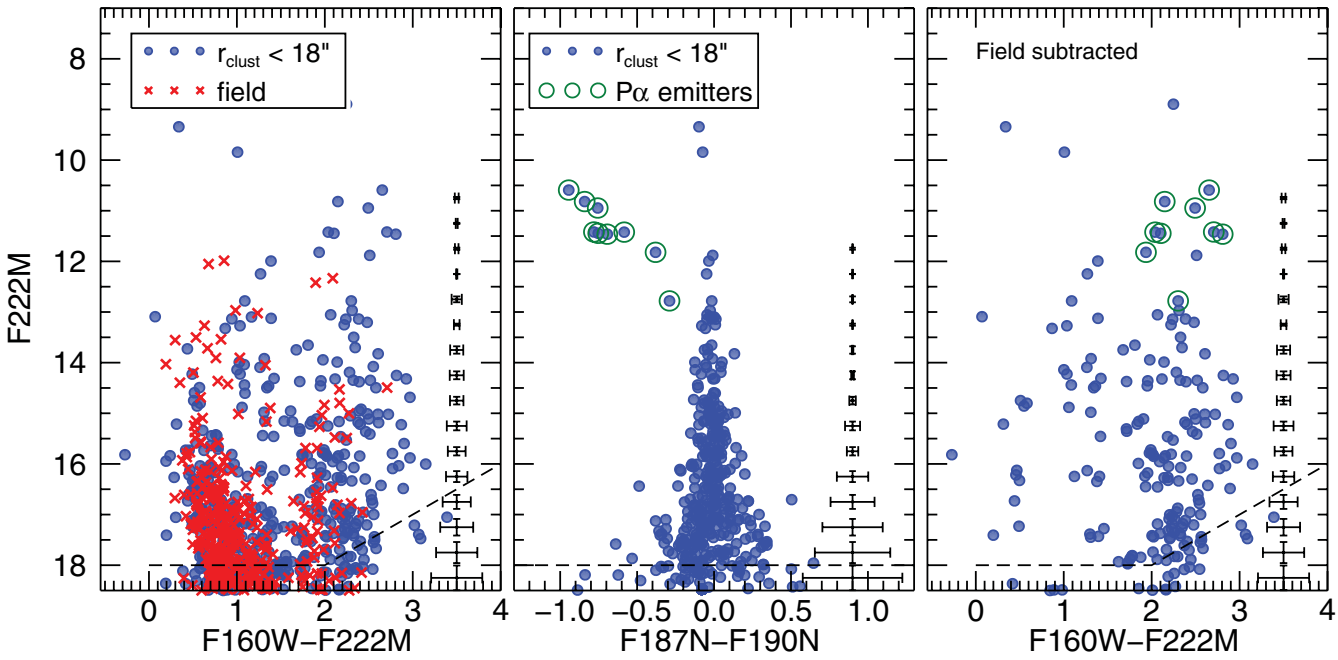

Figure 4. Colour–magnitude diagrams for Mc81 from the NICMOS photometry. Left: the stars within 15 arcsec of the cluster centre, which we define as the position of Mc81-2, compared to stars in a nearby control field of the same angular size. Centre: the Pα emission of stars within 15 arcsec of the cluster centre, as determined from the colour ($m_{187} - m_{190}$). Stars with significant emission are marked with green circles. Right: the same as the left panel, after the cluster field has been decontaminated of foreground stars using the control field observations. The long-dashed lines in each figure show the 50 per cent completeness levels.

Table 2. Astrometry and photometry of Mc81-1, plus the emission-line stars. Astrometry is taken from the *HST* observations and comparisons to 2MASS indicate that it is accurate to ∼1 arcsec.

ID	RA–Dec. (J2000)	m_{160}	m_{222}	m_{187}	m_{190}
1	16 40 29.83 −46 23 33.9	11.14	8.90	9.67	9.75
2	16 40 29.65 −46 23 29.1	13.25	10.59	10.69	11.63
3	16 40 30.08 −46 23 11.4	12.97	10.82	10.75	11.60
4	16 40 29.65 −46 23 28.7	13.44	10.95	11.15	11.91
5	16 40 28.35 −46 23 25.6	14.13	11.42	11.67	12.45
6	16 40 29.32 −46 23 11.6	13.46	11.42	11.56	12.14
7	16 40 29.60 −46 23 25.6	13.55	11.45	11.56	12.31
8	16 40 28.94 −46 23 27.1	14.27	11.46	11.95	12.65
9	16 40 29.32 −46 23 38.2	13.76	11.82	12.16	12.54
10	16 40 30.05 −46 23 24.3	15.08	12.78	13.41	13.70

an excess of stars at ($m_{160} - m_{222}$) $\simeq$ 2.3. The central panel shows the Pα excess stars. Stars with ($m_{187} - m_{190}$) colours <0.3 and $m_{222} > 13$ are defined as 'Pα emitters', as indicated in the plot. The locations and photometry of these stars are listed in Table 2.

Finally, the right-hand panel of Fig. 4 is the same as the left, but after the cluster field has been decontaminated of field stars using the data from the control field. We do this by eliminating stars from the cluster field that have a control-field star close by in colour–magnitude space. We set this limiting distance to be the larger of either the cluster field star's 1σ photometric errors, or 0.15 mag in colour and 0.1 mag in magnitude. We also set the restriction that no control-field star can eliminate more than one cluster field star. After decontamination, the cluster sequence at ($m_{160} - m_{222}$) $\simeq$ 2.3 becomes clearer, although there is still some scatter.

3.2 Spectroscopy

We now present the results of the spectroscopic observations. To classify the spectra, we refer to the spectral atlases of Hanson et al. (2005), Figer, McLean & Najarro (1997) and Crowther et al. (2006).

The spectra of the two brightest stars in Mc81 are shown in Fig. 5. The brighter star, Mc81-1, has relatively weak spectral features. The absorption lines of the hydrogen Brackett series, as well as some faint Mg II emission, are seen. We see no evidence of He I in either absorption or emission. The absence of He I suggests a spectral type later than ∼B5, while the emission lines of Mg II are indicative of a substantial stellar wind, more typical of supergiants. The 'ripples' seen between 2.05 and 2.08 μm are due to poor cancellation of the CO_2 absorption. For now, we assign a loose spectral type to this star of late-B/early-A supergiant. Taking the distance and extinction derived in Section 3.3, as well as the bolometric corrections tabulated by Blum et al. (2000) for spectral types B7–A2, we estimate the luminosity of the star to be in the range $\log(L/L_\odot) =$ 5.4–5.8, placing the star close to the empirical stellar luminosity limit at $\log(L/L_\odot) \simeq 5.9$ (Humphreys & Davidson 1979). Such stars are also seen in Westerlund 1 (Clark et al. 2005). The star's proximity to the Humphreys–Davidson limit suggests that the star may be in an unstable phase of evolution, such as a luminous blue variable or yellow hypergiant phase, although further spectroscopic and photometric monitoring would be required to verify this.

In contrast to Mc81-1, Mc81-3 has a spectrum rich in strong, broad emission lines. These lines can be attributed to H I, He I, He II and N III. The ratio of the He II 2.189 μm to the complex at 2.115 μm, as well as the absorption of He I 2.189 μm, allows us to tightly constrain the spectral type of this star to be WN 7–8.

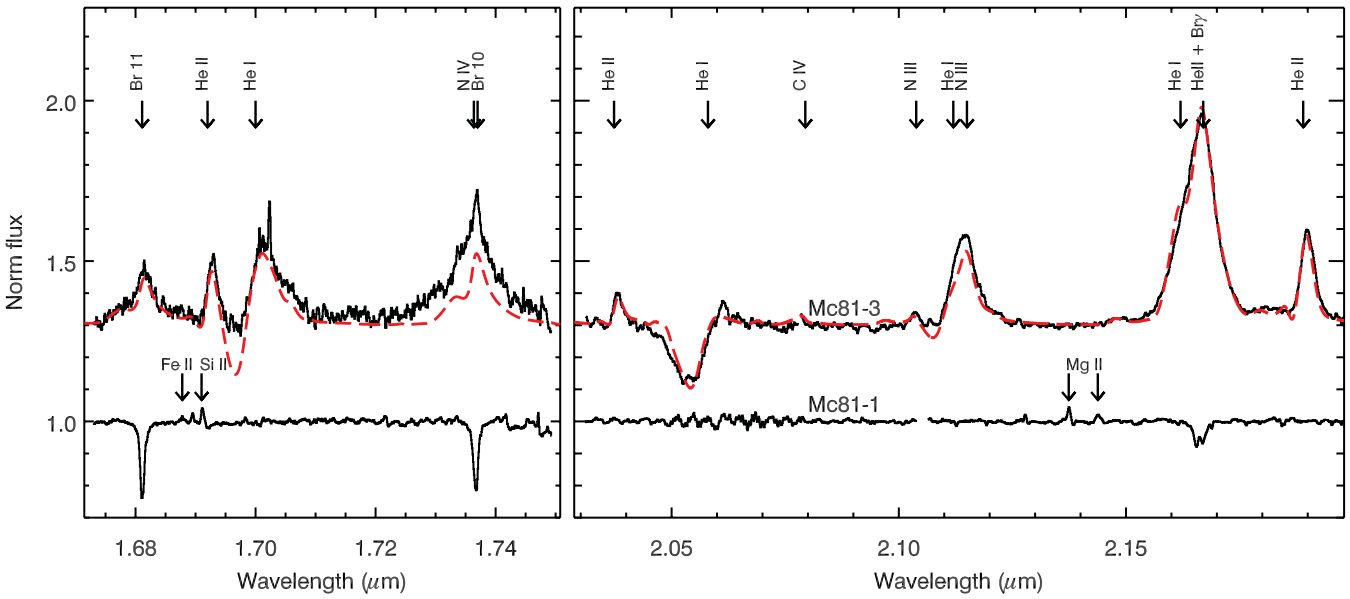

Figure 5. Spectra of the two stars observed. The wiggles seen at ∼2.05 μm are due to fringing on the detector, which we were unable to remove.

3.3 Extinction and distance

To calculate the extinction, we first determine the reddening of the cluster sequence from the right-hand panel of Fig. 4. The average colour of the stars in the decontaminated cluster field is $(m_{160} - m_{222}) = 2.3 \pm 0.3$. If we make the approximation that all main-sequence stars that we detect should have colours of approximately zero, the observed average colour is due to extinction. We can then determine the extinction from the following relation:

$$A_{\lambda_2} = \frac{E_{\lambda_1-\lambda_2}}{(\lambda_1/\lambda_2)^{\alpha} - 1}, \quad (1)$$

with $\lambda_1 = 1.60$ μm and $\lambda_2 = 2.22$ μm, i.e. the wavelengths of the NICMOS *F160W* and *F222M* filters. The parameter α has been studied by numerous authors in recent years (see e.g. Stead & Hoare 2009 and references therein), with the most contemporary measurements converging on $\alpha = -2.0 \pm 0.1$. This therefore implies that the extinction towards Mc81 is $A_{2.22} = 2.5 \pm 0.5$. Extrapolating this extinction to the optical is known to be highly uncertain, but we estimate $A_V = 45 \pm 15$.[3] Mc81 is therefore one of the most heavily reddened clusters known, with an extinction comparable to that of the Galactic Centre.

We estimate the distance to the cluster from the radial velocity of the surrounding molecular cloud. Caswell & Haynes (1987) studied the radio recombination line emission of the two clouds of ionized gas either side of the cluster, G338.4+0.2 and G338.4+0.1 (see Fig. 1), finding velocities relative to the local standard of rest of $v_{\rm lsr}$= −29 and −37 km s^{-1}, respectively. In addition, a number of massive young stellar objects (YSOs) and compact H II regions have been detected in the region by the Red MSX Source (RMS) survey (Hoare et al. 2005; Urquhart et al. 2007a,b), with an average radial velocity of $v_{\rm lsr} = -35.1 \pm 2.8$ km s^{-1}.

Comparing this average $v_{\rm lsr}$ to the Galactic rotation curve of Brand & Blitz (1993), using a Galactocentric distance of 7.6 ± 0.3 kpc and a rotational velocity of 214 ± 7 km s^{-1} (Kothes & Dougherty 2007 and references therein), we find near- and far kinematic distances of 3.8 and 11 kpc, respectively. To resolve the near/far ambiguity, we refer to the Southern Galactic Plane Survey (SGPS) of H I. These data were recently analysed by Lemiere et al. (2009), who found that for the two large H II regions G338.4+0.2 and G338.4+0.1, H I absorption components could be seen at several velocities up to the tangent point velocity of 130 km s^{-1}. This indicates that the H II regions, and by association the YSOs and the central star cluster, lie *beyond* the tangent point. From this, we conclude that the clusters lie at the far-side distance of 11 kpc. At this distance, the uncertainty is dominated by the systematic uncertainties in the Galactic rotation curve, which by its nature is difficult to quantify. However, if we assume that the system may have a peculiar velocity of up to ±20 km s^{-1} (Russeil 2003), this gives an uncertainty of ±2 kpc on this distance.

We can check this distance by calculating the absolute brightness of the WNL star and comparing to similar objects. Using the extinction calculated in the previous section and a distance of 11 ± 2 kpc, we find an absolute magnitude for Mc81-2 of $M_{222} = -7.1 \pm 0.6$. By comparison, Galactic WNL stars are typically found to have $M_K = 5.9 \pm 1.0$ (Crowther et al. 2006). Mc81-2 is therefore somewhat luminous for its spectral type, although it is within the errors for other Galactic WNL stars.

3.4 Cluster size

In Fig. 6, we illustrate the physical extent of the cluster. The figure shows the locations of all stars in the NICMOS field of view which are brighter than the 50 per cent completeness limit ($m_{222} < 17$), overlaid with stars that have colours consistent with the cluster (i.e. $m_{160} - m_{222} > 2.0$). The figure shows that there is a clear overdensity of stars at the coordinate centre (defined as the position of star Mc81-2).

To measure the size and morphology of this overdensity, we first made a map of the stellar density by dividing the field up into square bins of size 3 × 3arcsec^2 and counting the number of stars per bin. To reduce noise, this map was then smoothed, such that the effective resolution of the map was 6 arcsec (illustrated in the bottom corner

[3] Using the value of $\alpha = -1.53$ from Rieke & Lebofsky (1985), we find $A_{2.22} = 3.5 \pm 0.5$ and $A_V = 30 \pm 4$.

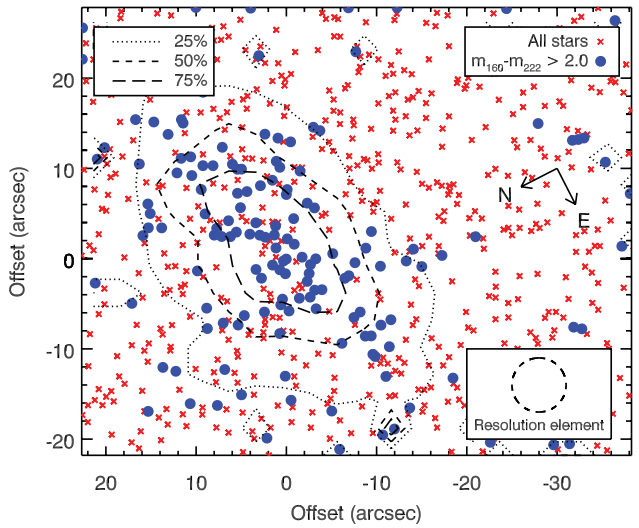

Figure 6. An illustration of the spatial extent of the cluster. Red crosses denote all stars in the NICMOS field brighter than the 50 per cent detection limit, while blue circles indicate stars with colours of $m_{160} - m_{222} > 2.0$. The contours indicate where the stellar density is 25, 50 and 75 per cent of the maximum. As the data were smoothed to make the contours, the circle on the bottom left shows the size of a resolution element.

of Fig. 6). This resolution size was chosen as a trade-off between spatial resolution and signal strength, though our results were robust to changes in this parameter. The ambient stellar density was found by computing the background level of this map using the GSFC IDL routine SKY. Finally, we computed isodensity contours in this map at percentiles of the maximum stellar density.

We defined the size of the cluster where the stellar density drops to 50 per cent of its maximum value, which we deem to be roughly equivalent to its half-light radius.[4] Once deconvolved with the effective spatial resolution, we find that the cluster has major and minor axes of 29×18 arcsec^2. At a distance of 11 kpc, this corresponds to 1.5×1.0 pc, and so is comparable to other young Galactic clusters which typically have diameters between 1 and 2 pc (e.g. Trumpler 14 and Westerlund 1; Figer 2008).

3.5 Quantitative spectral analysis

To model the WNL star in Mercer81 and estimate its physical parameters, we proceed as in Najarro et al. (2004, 2009). Briefly, we have used CMFGEN, the iterative, non-LTE line-blanketing method presented by Hillier & Miller (1998), which solves the radiative transfer equation in the comoving frame and spherical geometry for the expanding atmospheres of early-type stars. The model is prescribed by the stellar radius, R_*, the stellar luminosity, L_*, the mass-loss rate, $\dot{M}$, the velocity field, $v(r)$ (defined by the terminal wind speed v_∞ and the wind acceleration parameter β), the volume-filling factor characterizing the clumping of the stellar wind, $f(r)$, and elemental abundances. Hillier & Miller (1998, 1999) present a detailed discussion of the code. For the present analysis, we have assumed the atmosphere to be composed of H, He, C, N, O, Si, S, Fe and Ni. Observational constraints are provided by the H and K-band spectra of the stars and the dereddened F166W, F190N and F222M magnitudes.

[4] Ideally, to measure the half-light radius one would measure the cumulative surface brightness out to a distance where it becomes asymptotic. However, the field of view of our observations is too small to do this.

Table 3. Best-fitting model atmosphere parameters for Mc81-2.

Parameter	Value
$T_{\rm eff}$ (K)	36000 ± 1000
$T_{\tau=20}$ (K)	38000 ± 000
v_∞ (km s^{-1})	1350 ± 100
β	1.25
A(H/He)	0.75 ± 0.25
$\log(L/{\rm L}_\odot)$	6.3 ± 0.4
$\log(\dot{M}/{\rm M}_\odot\ {\rm yr}^{-1})$	-4.2 ± 0.2

Given the extreme sensitivity of the H- and K-band He I and He II line profile ratios in this parameter domain to changes in temperature, we estimate our errors in the temperature to be below 1000 K. Likewise, the relative strengths between the H and He lines constrain the H/He ratio to be within 0.5 and 1.0 by mass. The error on R_* and hence on L_* and $\dot{M}$ is dominated by those in the assumed distance and the slope of the extinction law.

The best-fitting model is overplotted in Fig. 5. The model provides a good fit to the features of the observed spectrum, with the exception of the Br10 line, which is blended with emission from N IV/C IV/O IV. This discrepancy is primarily due to the deficiencies in the CNO IV model atoms, the correction of which is beyond the scope of this work. The model's physical parameters are given in Table 3, and are typical for a late-type WN star. For completeness, we list the temperature at an optical depth of $\tau = 2/3$, which is comparable to the star's effective temperature; and the temperature at $\tau = 20$, which is comparable to the hydrostatic temperature of stellar structure models. In the following section, we use these results to estimate the age of Mc81-3 and therefore of the cluster itself.

3.6 Cluster age

In order to constrain the age of the cluster, we make a quantitative comparison between the physical properties of the WNL star Mc81-3 and the predictions of stellar evolutionary models. Assuming that the star and the host cluster are coeval, we can then estimate the cluster's age.

For this analysis, the models we have chosen are those of Meynet & Maeder (2000), which are optimized for massive stars. In our method, we linearly interpolate these mass tracks at intervals of 1 M$_\odot$ and 10^5 yr. For each point on each interpolated mass track, we then calculate the probability that there is a match between the mass track and Mc81-3, based on the star's luminosity $L_\star$, temperature T, and H/He ratio A(He) derived in the previous section. For the star's temperature, we use the temperature at an optical depth of $\tau = 20$, since this is more comparable to the hydrostatic temperature calculated by Meynet & Maeder (2000).

Fig. 7 shows the inter-related behaviour of the three variables $L_\star$, T and H/He for models with a range of initial stellar masses. We also plot the derived physical parameters of Mc81-3. The plot shows that, although the star's luminosity and H/He ratio place it on the 120 M$_\odot$ mass track, the temperature of the star (illustrated by the colour of the plotting symbol) more closely matches the 60 M$_\odot$ track.

We assume that the errors on $L_\star$, T and A(He) are Gaussian, and therefore the probability p of a match between Mc81-3 and the mass

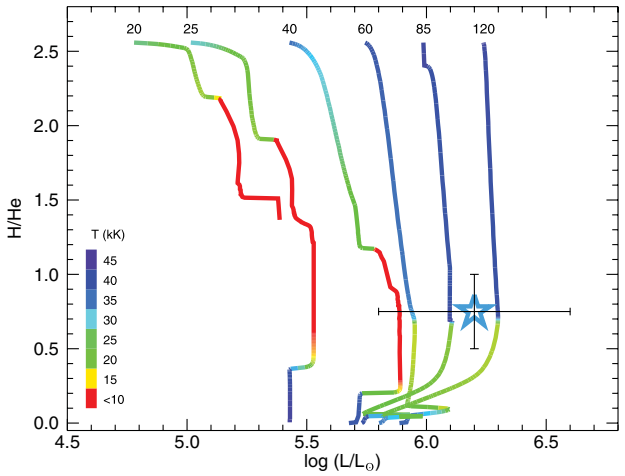

Figure 7. Geneva evolutionary tracks from Meynet & Maeder (2000). The *x*- and *y*-axes plot the H/He mass fraction and luminosity, respectively, while the colour of the track indicates the effective temperature at that point in the evolution. The initial mass of each track is indicated at the top. Our derived parameters for Mc81-3 are indicated by the position and colour of the star symbol. Although the symbol intercepts the 120 $M_\odot$ track in the (H/He)–*L* space, the temperature of the star means that the best fit is actually with the 60 $M_\odot$ track (see also Fig. 8).

track of initial mass m at time t is given by

$$p(m,t) = \prod_i \exp\left(-\frac{(\mathcal{M}_i - \mathcal{O}_i)^2}{2\sigma^2_{\mathcal{O}_i}}\right), \quad (2)$$

where $\mathcal{O}$ is the observed quantity [either $L_\star$, T or A(He)], $\sigma_\mathcal{O}$ is its associated uncertainty, and $\mathcal{M}$ is the corresponding quantity predicted by the model mass track. Each term is therefore weighted by its associated uncertainty.

In Fig. 8 we plot how the probability varies across the 2D plane of mass and stellar age for the rotating models of Meynet & Maeder (2000). The maximum probability ($p = 0.75$) is obtained for an initial mass of $M_\star = 62$ $M_\odot$ and an age of 3.7 Myr. The morphology of the isoprobability contours is highly non-Gaussian, so for the experimental uncertainty we cannot simply compute the standard

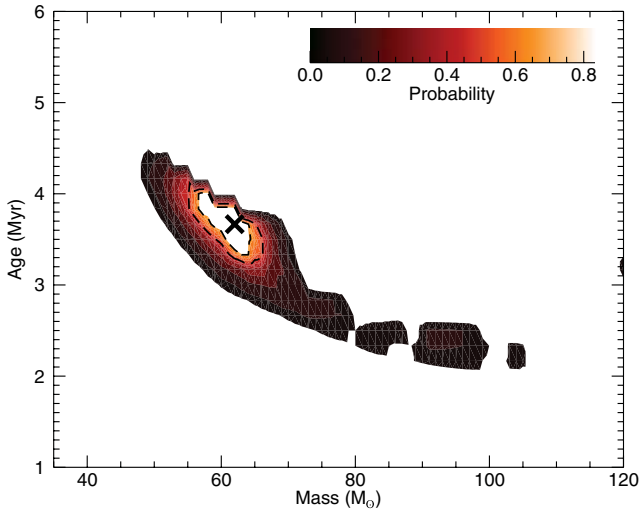

Figure 8. Probability map derived from fitting stellar mass tracks to the luminosity, temperature and H/He of the WNL star Mc81-3. The age and initial mass of the best-fitting model are indicated by the cross, and isoprobability contours are drawn at 67 and 50 per cent.

deviation. Instead, we take the isoprobability contour at 50 per cent and determine the minimum and maximum values of mass and age for that contour. In this way, for Mc81-3 we find $M_\star = 62^{+6}_{-7}$ $M_\odot$ and an age of $3.7^{+0.4}_{-0.5}$ Myr. Using the non-rotating versions of the same stellar evolution models produces a slightly different morphology to the probability distribution, with a reduced probability, but with a best-fitting age and mass that do not differ significantly from those derived using the rotating models.

The value we obtain for Mc81-3's age can be understood through a simple qualitative analysis of the star's parameters. The high luminosity clearly favours high initial masses and therefore a young age. In addition, the He enrichment indicates an object which is in an advanced evolutionary state, and so older than ∼2 Myr, but younger than the total lifetime of a high-mass star, and therefore younger than ∼5 Myr.

3.6.1 The impact of binary evolution on our derived cluster age

Throughout this analysis we have assumed that Mc81-3 has evolved as a single star. However, there is the possibility that the star is in an interacting binary: both Landi et al. (2006) and Funk et al. (2007) have detected X-ray emission from the centre of the cluster, which could be evidence of a colliding wind binary system. As shown by Eldridge (2009) for the case of γ^2 Vel, including the effects of binary evolution in the analysis can alter the derived age of a star.

In the case of Mc81-3, the its high luminosity places a strong constraint on the initial mass of the star, and hence on the upper limit of its age. Though binary evolution can affect the surface abundances and temperature of a star, and prolong its lifetime, it is unlikely to increase the star's maximum luminosity by more than ∼0.1 dex, which is governed primarily by the initial stellar mass (all other parameters being equal) (Eldridge, Izzard & Tout 2008). An exception to this would be if two stars merged to produce a completely rejuvenated and more massive star. In the absence of any evidence for such an event in the history of Mc81-3, we maintain that the upper limit to the star's age is that derived in the previous paragraph.

The lower limit to the cluster age may be reduced if Mc81-3 is in an interacting binary system. Mass transfer from the primary to the secondary star may speed up the rate at which H is depleted from the primary's surface. In this case, we would underestimate the stellar (and hence cluster) age by using single-star evolution models in our analysis.

However, a simple morphological analysis of the nebula surrounding Mc81 and a comparison to similar systems serves as a sanity check on our age estimate. The cluster is located at the centre of a cavity, which was presumably evacuated by the winds, ionizing radiation and SNe explosions of the most massive stars in the cluster. At the periphery of the cavity, evidence of further generations of star formation is seen, which may or may not have been triggered by a feedback from the cluster. This morphology is reminiscent of other cluster+nebula systems such as G305, NGC 3603 and NGC 346. Ages of these other systems are commonly found to be 2–4 Myr (Bouret et al. 2003; Harayama, Eisenhauer & Martins 2008; Davies, Clark & Others 2011a) and therefore are consistent with our estimate for Mc81.

3.7 Cluster mass

For the cluster mass, it is difficult to make an accurate estimate without further spectroscopy of the stars in the cluster. We can however

make a rough estimate of the cluster mass from the emission-line stars. If we assume that *all* the nine strong Pα emitters listed in Table 2 are WR stars, then since the age we derive for Mc81 is roughly the same as that of Westerlund 1 (Wd1) (3–5 Myr; Crowther et al. 2006; Brandner et al. 2008) which has 27 WR stars, this suggests that Mc81 may be a factor of $\sim$3 less massive than Wd1. As most estimates of Wd1's mass are around $10^5\,M_\odot$ (Clark et al. 2005; Brandner et al. 2008), this implies that the mass of Mc81 is a few $\times 10^4\,M_\odot$. We stress however that this is only an order-of-magnitude estimate; a more precise measurement of the cluster mass awaits further analysis of its stellar population.

4 DISCUSSION

4.1 Location in the Galaxy

With the many recent discoveries of young star clusters in the Galaxy, we can now build up a picture of the Galaxy's recent cluster formation. In Fig. 9 we plot the locations of all known young Galactic clusters with distances from the Sun greater than $\sim$2 kpc. All clusters in the plot are thought to have masses in excess of $10^3\,M_\odot$ and ages $\lesssim$20 Myr. The references for each data point are listed in Table 4. We have colour coded each data point according to its visual extinction, which we have calculated in a homogeneous way from each cluster's $E(H-K)$, measured either from the references listed in Table 4 or from 2MASS photometry, and an extinction law slope of $\alpha = -2.0$ (see Section 3.3).

Fig. 9 shows that there are now a significant number of reddened star clusters known at Galactic longitudes between $10 \gtrsim l \gtrsim 50$. This line of sight corresponds to the tangent of the Scutum-Crux arm, as well as the near end of the Galactic Bar (Benjamin et al. 2005). Since one would expect the star formation rate to be comparatively high in this location of the Galaxy, it is also reasonable to expect it to be rich in young star clusters. Indeed, the region hosts five known YMCs, plus a substantial field population of red supergiants, indicating a starburst episode of $\sim 10^6\,M_\odot$ around 20 Myr ago (Garzon et al. 1997; López-Corredoira et al. 1999; Figer et al. 2006; Davies et al. 2007; Clark et al. 2009b; Negueruela et al. 2010, 2011).

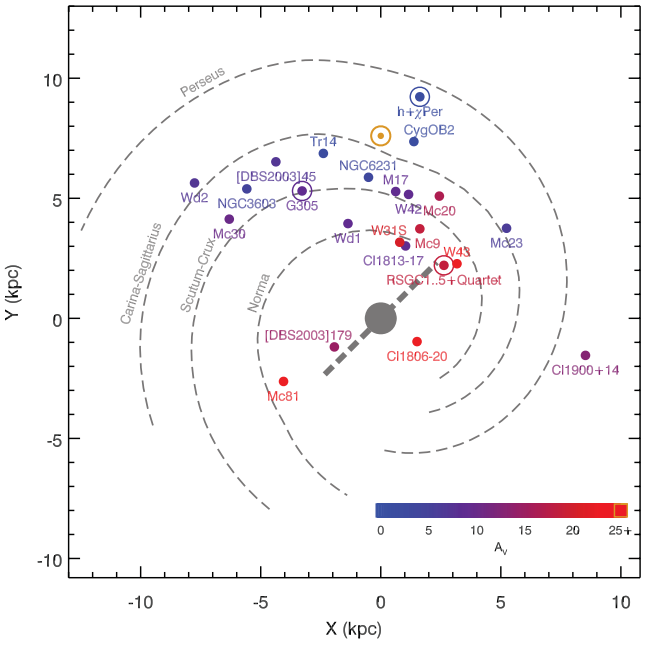

Figure 9. Top down view of the Galaxy, showing the locations of young star clusters. The colour of the plotting symbols indicate the extinction of each cluster, derived from their NIR colours and assuming an extinction law slope of -2.0. The spiral arms are those defined by Cordes & Lazio (2002). Sites of multiple star clusters are indicated by a filled circle surrounded by an open circle.

Table 4. Young star clusters in the Galactic plane. The visual extinction A_V has been determined homogeneously from each cluster's IR colour excess $E(H-K)$, using the relation $A_V \simeq 19 \times E(H-K)$, which follows from an NIR extinction law with slope $\alpha = -2.0$. See the referenced papers for detailed error analysis on the distances.

Cluster	l (°)	D (kpc)	A_V	Reference
Cl 1806–20	10.0	8.7	30.3	1
W31S	10.1	4.5	20.9	2
Cl 1813–17	12.7	4.7	9.5	3
M17	15.0	2.4	9.5	4
Mc9	22.8	4.2	19.0	5
W42	25.4	2.7	9.5	6
RSGC1 to 5, Quartet	26.0	6.0	19.0	7–12
W43	30.8	6.2	39.8	13
Cl 1900+14	43.0	12.5	13.3	14
Mc20	44.2	3.5	17.1	12
Mc23	53.7	6.5	6.6	15
Cyg OB2	80.2	1.4	6.0	16–17
h+χ Per	135.0	2.3	1.9	18
[DBS2003]45	283.9	4.5	7.6	19
Westerlund 2	284.2	8.0	7.6	20
Trumpler 14	287.0	2.5	2.5	21
NGC 3603	291.6	6.0	4.7	22
Mc30	298.8	7.2	10.5	23
Danks 1 and 2	305.0	4.0	9.5	24
Mc81	338.4	11.0	41.7	This work
Westerlund 1	339.5	3.9	9.5	25
NGC 6231	343.5	1.8	3.8	26
[DBS2003]179	347.6	9.0	15.2	27; this work

References. 1: Bibby et al. (2008); 2: Blum et al. (2001); 3: Messineo et al. (2008); 4: Hanson, Conti & Rieke (1996); 5: Messineo et al. (2010); 6: Blum et al. (2000); 7: Davies et al. (2008); 8: Davies et al. (2007); 9: Clark et al. (2009b); 10: Negueruela et al. (2010); 11: Negueruela et al. (2011); 12: Messineo et al. (2009); 13: Blum et al. (1999); 14: Davies et al. (2009); 15: Hanson et al. (2010); 16: Hanson (2003); 17: Wright et al. (2010); 18: Currie et al. (2010); 19: Zhu et al. (2009); 20: Rauw et al. (2007); 21: Ascenso et al. (2007); 22: Harayama et al. (2008); 23: Kurtev et al. (2007); 24: Davies et al. (2011a); 25: Kothes & Dougherty (2007); 26: Raboud, Cramer & Bernasconi (1997); 27: Borissova et al. (2008).

However, less is known about the opposite side of the Galactic Centre and far end of the Bar. There are two possible reasons for this: first, the larger distance, high extinction and the larger number of foreground stars (due to the intervening Galactic bulge) make it more difficult to pick out clusters in by-eye searches. Indeed, it is unlikely that Mc81 would have been found were it not for the four bright foreground stars (see Section 3.1). Secondly, the fact that no star clusters are known in this direction means that investigators are less likely to search this region. This is in contrast to the near end of the Bar, where the initial discovery of the cluster RSGC1 in this region by Figer et al. (2006) led to the subsequent discoveries of a further four clusters within the same complex.[5]

[5] Though RSGC1 and RSGC2 were first recognized as associations of stars by Bica et al. (2003) and Stephenson (1990) respectively, the nature of each cluster was not understood until later.

From our distance estimate of Mc81, we can place this cluster close to where we suppose the far end of the Bar may be, assuming an azimuthal angle of 44° and a bar length of 4.4 kpc (Benjamin et al. 2005). Another nearby cluster, which may too trace the end of the Bar, is [DBS2003]179. The distance to this cluster is not well known, and is based on spectrophotometric distance estimates for stars with unknown luminosity classes (Borissova et al. 2008). We have reassessed the distance to this cluster using a methodology similar to that presented here for Mc81. Specifically, we assume that the cluster is physically associated with its nearby molecular cloud, and use the massive YSOs detected in the cloud to determine the systemic radial velocity. We then use the SGPS survey (McClure-Griffiths et al. 2005) to measure the velocity spectrum of the intervening H I gas to resolve the distance ambiguity. The average radial velocities of the YSOs ($v_{\rm lsr} = -36 \pm 3\,{\rm km\ s^{-1}}$), combined with the H I absorption which is seen up to tangent-point velocities of 130 km s^{-1}, give a far-side kinematic distance of 9 kpc, again with a ± 2 km s^{-1} uncertainty to allow for deviations from the Galactic rotation curve (see Section 3.3). This is within the errors of the spectrophotometric distance of 7.9 kpc derived by Borissova et al. (2008).

These two clusters – Mc81 and [DBS2003]179 – are then the first young star clusters to be discovered in this region of the Galaxy. In addition to these clusters, the detection of a group of giant H II regions, one of which is G338.4+0.1 (Russeil 2003), suggests that this region may be an active star formation site, similar to the region of the Scutum–Crux tangent at the opposite end of the Bar. Therefore, future targeted surveys of this region may unearth a number of other such objects.

4.2 Association with HESS 1640–465

As noted in Section 2, the Mc81 cluster is located only a few arcminutes from the TeV source HESS 1640–465, which is likely to be powered by a neutron star. If the two were associated, it would allow us to estimate the initial mass of the neutron star's progenitor. Here we discuss the possible association between these two objects.

HESS 1640–465 is known to have a counterpart source at GeV energies (Slane et al. 2010), and in the X-ray, detected by the *Swift*, *XMM–Newton* and *Chandra* (Landi et al. 2006; Funk et al. 2007; Lemiere et al. 2009). An analysis of the *XMM–Newton* X-ray spectrum yielded a column density of $n_{\rm H} = 6.1^{+2.1}_{-0.6} \times 10^{22}\,{\rm cm^{-2}}$ or $3.6^{+1.1}_{-0.8} \times 10^{22}\,{\rm cm^{-2}}$, depending on the use of a power-law or absorbed blackbody model (Funk et al. 2007). However, Lemiere et al. (2009) analysed the *Chandra* data and found that they required a higher column density of $1.4 \times 10^{23}\,{\rm cm^{-2}}$ to fit the data. Assuming a standard calibration between $n_{\rm H}$ and optical extinction A_V of $n_{\rm H} = 1.8 \times 10^{21} A_V\,{\rm cm^{-2}}$ (Predehl & Schmitt 1995), this implies a visual extinction of between 20 and 70 mag, depending on the model for the X-ray emission. Though the errors are large, this is consistent with our measurement of the extinction to the cluster of $A_V = 45 \pm 15$.

From this evidence, it seems likely that HESS 1640–465 is associated with the G338.4+0.1 H II region surrounding Mc81. However, its connection with the cluster itself is not clear. If the central source of HESS 1640–465 is a neutron star (as seems likely), and the progenitor *was* born with the cluster but was ejected, there are two possibilities: either the progenitor was dynamically ejected from the cluster or it received a kick from the SN. The location of HESS 1640–465 at the centre of SNR 338.3+0.0 (Green 2004) provides circumstantial evidence against the latter explanation, since this suggests that the progenitor exploded close to its present location. If the progenitor formed with the cluster but was ejected at a time $t_{\rm ej}$ ago, the ejection velocity is $\simeq 20(t_{\rm ej}/{\rm Myr})\,{\rm km\ s^{-1}}$ (assuming a projected distance of 22 pc). Therefore, it is entirely plausible that the progenitor star formed along with the rest of the stars in Mc81 and was dynamically ejected during the formation of the cluster.

Finally, there is the possibility that HESS 1640–465 formed out of the same molecular cloud as Mc81, and at a similar time, but that the two formed independently of each other. The morphology of the G338.4 region suggests inside-out star formation, with the ∼3-Myr-old cluster in the centre and a series of YSOs and ultra compact (UC) H II regions at the periphery of the surrounding cavity, which have ages of a few $\times 10^5$ yr (Davies et al. 2011b). The location of HESS 1640–465 does not fit this picture, since the progenitor star must have formed at least 2 Myr ago, that is, before the first SNe occurred in Mc81. However, there are other known instances of 'multi-seeded' star formation where collapse occurs at multiple causally unrelated sites across the host giant molecular cloud (GMC) (e.g. W51, Clark et al. 2009a).

In summary, we conclude that HESS 1640–465 is likely associated with the star-formation region of G338.4+0.1. However, we are unable to make a definitive association with the star cluster Mc81, and so we are unable to use the age of the cluster to estimate the mass of the neutron star's progenitor, as we were in the cases of e.g. RSGC1 and Cl 1900+14 (Davies et al. 2008, 2009).

5 SUMMARY

We have provided an NIR photometric and spectroscopic investigation of the candidate star cluster Mercer 81 (Mc81). We find that that a highly reddened ($A_V = 45 \pm 15$) cluster exists in the field identified by Mercer et al. (2005), but the four bright stars at the centre of the field are unrelated foreground objects. The cluster is located at the centre of a cavity in a large H IIregion in the direction of G338.4+0.1, with evidence of ongoing star formation in the periphery of the cloud. Our analysis of the cluster has revealed nine stars with strong Pα emission, one of which we identify spectroscopically as a late-type N-rich WR star (WNL), in addition to a luminous early A-type supergiant. Through detailed modelling of the WNL star's spectrum, we estimate an age of $3.7^{+0.4}_{-0.5}$ Myr for the cluster. Assuming that the stars with strong line emission are WR stars, we have made an order-of-magnitude estimate of the cluster's mass of $\gtrsim 10^4\,{\rm M_\odot}$.

From a kinematic analysis of the host cloud, we obtain a distance of 11 ± 2 kpc to the host star-forming complex. Our distance estimate therefore places the G338.4+0.1 complex in the same region of the Galaxy as the far end of the Galactic Bar. The recent detection of another star cluster close to this location, as well as other giant H II regions, suggest that this region of the Galaxy may be as active in star formation as the opposite end of the Bar, where a $\sim 10^6\,{\rm M_\odot}$ starburst event is known to have occurred in the last ∼20 Myr. A targeted search of the far end of the Bar will likely uncover many more young star clusters, although the high extinction, large distance and dense stellar field of the intervening Galactic bulge will mean that such a search will require considerable observational effort.

ACKNOWLEDGMENTS

We thank the anonymous referee for comments and suggestions that helped us improve the paper. BD is supported by a fellowship from the Royal Astronomical Society. This work is in part based on observations made with the NASA/ESA *Hubble Space Telescope*, obtained at the Space Telescope Science Institute, which is operated

by the Association of Universities for Research in Astronomy, Inc., under NASA contract NAS 5-26555. These observations are associated with programme #11545. Support for programme #11545 was provided by NASA through a grant from the Space Telescope Science Institute, which is operated by the Association of Universities for Research in Astronomy, Inc., under NASA contract NAS 5-26555. This work is in part based on observations collected at the European Organisation for Astronomical Research in the Southern Hemisphere, Chile, under programme number 083.D-0765(A). Financial support from the Spanish Ministerio de Ciencia e Innovación under projects AYA2008-06166-C03-02 and AYA2010-21697-C05-01 is acknowledged.

REFERENCES

Aharonian F. et al., 2005, Sci, 307, 1938
Aharonian F. et al., 2007, A&A, 467, 1075
Alonso-Herrero A., Rieke G. H., Rieke M. J., Scoville N. Z., 2002, AJ, 124, 166
Ascenso J., Alves J., Vicente S., Lago M. T. V. T., 2007, A&A, 476, 199
Bastian N., Gieles M., Efremov Y. N., Lamers H. J. G. L. M., 2005, A&A, 443, 79
Benjamin R. A. et al., 2003, PASP, 115, 953
Benjamin R. A. et al., 2005, ApJ, 630, L149
Bibby J. L., Crowther P. A., Furness J. P., Clark J. S., 2008, MNRAS, 386, L23
Bica E., Dutra C. M., Soares J., Barbuy B., 2003, A&A, 404, 223
Blum R. D., Damineli A., Conti P. S., 1999, AJ, 117, 1392
Blum R. D., Conti P. S., Damineli A., 2000, AJ, 119, 1860
Blum R. D., Damineli A., Conti P. S., 2001, AJ, 121, 3149
Bock D. C.-J., Large M. I., Sadler E. M., 1999, AJ, 117, 1578
Borissova J. et al., 2008, A&A, 488, 151
Borissova J. et al., 2011, A&A, 532, A131
Bouret J.-C. et al., 2003, ApJ, 595, 1182
Brand J., Blitz L., 1993, A&A, 275, 67
Brandner W. et al., 2008, A&A, 478, 137
Caswell J. L., Haynes R. F., 1987, A&A, 171, 261
Clark J. S., Negueruela I., Crowther P. A., Goodwin S. P., 2005, A&A, 434, 949
Clark J. S. et al., 2008, A&A, 477, 147
Clark J. S. et al., 2009a, A&A, 504, 429
Clark J. S. et al., 2009b, A&A, 498, 109
Cordes J. M., Lazio T. J. W., 2002, arXiv (astro-ph/0207156v3)
Cotera A. S. et al., 1996, ApJ, 461, 750
Crowther P. A., Hadfield L. J., Clark J. S., Negueruela I., Vacca W. D., 2006, MNRAS, 372, 1407
Currie T. et al., 2010, ApJS, 186, 191
Davies B. et al., 2007, ApJ, 671, 781
Davies B. et al., 2008, ApJ, 676, 1016
Davies B. et al., 2009, ApJ, 707, 844
Davies B. et al., 2011a, MNRAS, doi:10.1111/j.1365.2966.2011.19736.x, preprint (arXiv:1109.0314)
Davies B. et al., 2011b, MNRAS, 416, 972
De Marchi G. et al., 2011, ApJ, 739, 27
Diolaiti E. et al., 2000, A&AS, 147, 335
Dutra C. M., Bica E., Soares J., Barbuy B., 2003, A&A, 400, 533
Eldridge J. J., 2009, MNRAS, 400, L20
Eldridge J. J., Izzard R. G., Tout C. A., 2008, MNRAS, 384, 1109
Figer D. F., 2008, in Bresolin F., Crowther P. A., Puls J., eds, IAU Symp. 250, Massive Stars as Cosmic Engines. Cambridge Univ. Press, Cambridge, p. 247
Figer D. F., McLean I. S., Najarro F., 1997, ApJ, 486, 420
Figer D. F. et al., 1999, ApJ, 525, 750
Figer D. F. et al., 2006, ApJ, 643, 1166
Froebrich D., Scholz A., Raftery C. L., 2007, MNRAS, 374, 399
Fuchs Y. et al., 1999, A&A, 350, 891
Funk S. et al., 2007, ApJ, 662, 517
Garzon F. et al., 1997, ApJ, 491, L31
González Delgado R. M., Pérez E., 2000, MNRAS, 317, 64
Green D. A., 2004, Bull. Astron. Soc. India, 32, 335
Hanson M. M., 2003, ApJ, 597, 957
Hanson M. M., Conti P. S., Rieke M. J., 1996, ApJS, 107, 281
Hanson M. M., Kudritzki R.-P., Kenworthy M. A., Puls J., Tokunaga A. T., 2005, ApJS, 161, 154
Hanson M. M. et al., 2010, A&A, 516, A35
Harayama Y., Eisenhauer F., Martins F., 2008, ApJ, 675, 1319
Hillier D. J., Miller D. L., 1998, ApJ, 496, 407
Hillier D. J., Miller D. L., 1999, ApJ, 519, 354
Hoare M. G. et al., 2005, in Cesaroni R., Felli M., Churchwell E., Walmsley M., eds, IAU Symp 227, Massive Star Birth: A Crossroads of Astrophysics. Cambridge Univ. Press, Cambridge, p. 370
Humphreys R. M., Davidson K., 1979, ApJ, 232, 409
Ivanov V. D., Borissova J., Pessev P., Ivanov G. R., Kurtev R., 2002, A&A, 394, L1
Konstantopoulos I. S. et al., 2009, ApJ, 701, 1015
Kothes R., Dougherty S. M., 2007, A&A, 468, 993
Kurtev R., Borissova J., Georgiev L., Ortolani S., Ivanov V. D., 2007, A&A, 475, 209
Landi R. et al., 2006, ApJ, 651, 190
Lemiere A., Slane P., Gaensler B. M., Murray S., 2009, ApJ, 706, 1269
López-Corredoira M. et al., 1999, AJ, 118, 381
Martins F. et al., 2007, A&A, 468, 233
Martins F. et al., 2008, A&A, 478, 219
McClure-Griffiths N. M. et al., 2005, ApJS, 158, 178
Mercer E. P. et al., 2005, ApJ, 635, 560
Messineo M. et al., 2008, ApJ, 683, L155
Messineo M. et al., 2009, ApJ, 697, 701
Messineo M. et al., 2010, ApJ, 708, 1241
Meynet G., Maeder A., 2000, A&A, 361, 101
Minniti D. et al., 2010, Nat, 15, 433
Moorwood A. et al., 1998, Messenger, 94, 7
Najarro F., Figer D. F., Hillier D. J., Kudritzki R. P., 2004, ApJ, 611, L105
Najarro F., Figer D. F., Hillier D. J., Geballe T. R., Kudritzki R. P., 2009, ApJ, 691, 1816
Negueruela I., González-Fernández C., Marco A., Clark J. S., Martínez-Núñez S., 2010, A&A, 513, A74
Negueruela I., González-Fernández C., Marco A., Clark J. S., 2011, A&A, 528, A59
Predehl P., Schmitt J. H. M. M., 1995, A&A, 293, 889
Price S. D., Egan M. P., Carey S. J., Mizuno D. R., Kuchar T. A., 2001, AJ, 121, 2819
Raboud D., Cramer N., Bernasconi P. A., 1997, A&A, 325, 167
Rauw G. et al., 2007, A&A, 463, 981
Rieke G. H., Lebofsky M. J., 1985, ApJ, 288, 618
Russeil D., 2003, A&A, 397, 133
Skrutskie M. F. et al., 2006, AJ, 131, 1163
Slane P. et al., 2010, ApJ, 720, 266
Smith N., 2006, MNRAS, 367, 763
Stead J. J., Hoare M. G., 2009, MNRAS, 400, 731
Stephenson C. B., 1990, AJ, 99, 1867
Urquhart J. S. et al., 2007a, A&A, 461, 11
Urquhart J. S. et al., 2007b, A&A, 474, 891
Vrba F. J. et al., 2000, ApJ, 533, L17
Westerlund B. E., 1987, A&AS, 70, 311
Wright N. J. et al., 2010, ApJ, 713, 871
Zhu Q., Davies B., Figer D. F., Trombley C., 2009, ApJ, 702, 929

This paper has been typeset from a TEX/LATEX file prepared by the author.